PHYSICAL REVIEW D **78,** 114508 (2008)

# Lattice study of the $N$-$P_{11}$ transition form factors

Huey-Wen Lin,* Saul D. Cohen, Robert G. Edwards, and David G. Richards
*Thomas Jefferson National Accelerator Facility, Newport News, Virginia 23606, USA*
(Received 2 April 2008; published 29 December 2008)

Experiments at Jefferson Laboratory, MIT-Bates, LEGS, Mainz, Bonn, GRAAL, and Spring-8 offer new opportunities to understand in detail how nucleon resonance ($N^*$) properties emerge from the nonperturbative aspects of QCD. Preliminary data from CLAS Collaboration, which cover a large range of photon virtuality $Q^2$, show interesting behavior with respect to $Q^2$ dependence: in the region $Q^2 \leq 1.5$ GeV$^2$, both the transverse amplitude $A_{1/2}(Q^2)$ and the longitudinal amplitude $S_{1/2}(Q^2)$ decrease rapidly. In this work, we attempt to use first-principles lattice QCD (for the first time) to provide a model-independent study of the transition form factor between the nucleon and its first radially excited state.

DOI: 10.1103/PhysRevD.78.114508 PACS numbers: 11.15.Ha, 12.38.Gc, 13.40.Gp, 14.20.Gk

## I. INTRODUCTION

Lattice QCD has successfully provided many experimental quantities from first-principles calculations; however, its success has mostly been restricted to measurements of ground-state quantities. Lattice measurements of excited states could contribute, for example, to hadron spectroscopy, where there are many poorly known states which require theoretical input to be identified. At the EBAC at Jefferson Lab, dynamical reaction models have been developed to interpret extracted $N^*$ parameters in terms of QCD [1,2].

Among these excited nucleon states, the nature of the Roper resonance, $N(1440)$ or $N'$, has been the subject of interest since its discovery in the 1960s. It is quite surprising that the nucleon's excited-state mass is lower than its opposite-parity partner, a phenomenon never observed in meson systems. There are several interpretations of the Roper state, for example, as the hybrid state that couples predominantly to QCD currents with some gluonic contribution [3], or as a five-quark (meson-baryon) state [4]. Some earlier quenched lattice QCD calculations, e.g. Refs. [5–10], found a spectrum inverted with respect to experiment, with $N'$ heavier than the opposite-parity state $S_{11}$. However, Ref. [11], in which larger lattice box and lighter pion masses are used, found a rapid crossover of the first positive- and negative-parity excited nucleon states close to the chiral limit. The lattice study has not ruled out that the Roper is the first radially excited state of the nucleon, and this is our assumption in this work.

The new data provided from experiments at Jefferson Laboratory, MIT-Bates, LEGS, Mainz, Bonn, GRAAL, and Spring-8 offer a new opportunity to understand in detail how nucleon resonance ($N^*$) properties emerge from the nonperturbative aspects of QCD. For example, the extraction of the $\gamma N \to N^*$ transition form factors could help us to understand the dynamical origins of the confinement of constituent quarks and the associated meson cloud. There are various QCD-based hadron models, such as the well-developed constituent quark model [12,13] and the covariant model based on Dyson-Schwinger equations [14].

Understanding of the true nature of the Roper resonance may be most easily gained by studying its structure and form factors, such as the nucleon-Roper transition. The CLAS Collaboration [15–19] has studied such transitions induced by electron scattering over a large range of intermediate photon virtuality $Q^2$. In the region $Q^2 \leq 1.5$ GeV$^2$, both the transverse amplitude $A_{1/2}(Q^2)$ and the longitudinal amplitude $S_{1/2}(Q^2)$ drop rapidly in magnitude. This is well described in relativistic quark models with light-cone dynamics, and the sign is consistent with the nonrelativistic version. However, in the low-$Q^2$ region, $A_{1/2}(Q^2)$ becomes negative; this is not understood within constituent quark models and requires inclusion of meson degrees of freedom [13,19]. A model-independent study of these quantities from lattice QCD will serve as valuable help to phenomenologists in analyzing experimental data and will provide better theoretical ground for understanding low-$Q^2$ physics.

## II. THE $\gamma^* N \to P_{11}$ FORM FACTORS

From Lorentz symmetry, we expect the matrix element between any spin-1/2 positive-parity nucleon states, $N_1$ and $N_2$, to have the following general form:

$$\langle N_2(p')|V_\mu|N_1(p)\rangle_\mu(q) = \overline{u}_{N_2}(p')\left[F_1^*(q^2)\left(\gamma\mu - \frac{q\mu}{q2}\not{q}\right) + \sigma_{\mu\nu}q^\nu \frac{F_2^*(q^2)}{M_{N_1}+M_{N_2}}\right] \times u_{N_1}(p)e^{-iq\cdot x}, \quad (1)$$

where $\sigma_{\mu\nu} = \frac{1}{2}[\gamma_\mu, \gamma_\nu]$, $q = p' - p$, and the equation of motion is used to simplify $-q_\mu\gamma^\mu = M_{N_2} - M_{N_1}$.

So that we can compare our extracted form factors with experimental results, we express the experimentally measured helicity amplitudes $A_{1/2}$ and $S_{1/2}$ in terms of the

*hwlin@jlab.org

 

transition form factors $F^*_{1,2}$ through

$$A_{1/2}(Q^2) = k_A(Q^2)G_M(Q^2),$$
$$S_{1/2}(Q^2) = k_S(Q^2)G_E(Q^2) \tag{2}$$

with $Q^2 = -q^2$,

$$k_A(Q^2) \equiv \sqrt{2\pi\alpha \frac{Q^2 + (M_{N_1} - M_{N_2})^2}{M_{N_2}(M^2_{N_1} - M^2_{N_2})}}, \tag{3}$$

$$k_S(Q^2) \equiv k_A(Q^2)\frac{M_{N_1} + M_{N_2}}{2\sqrt{2}Q^2 M_{N_1}} \times \sqrt{Q^2 + (M_{N_1} - M_{N_2})^2}\sqrt{Q^2 + (M_{N_1} + M_{N_2})^2}, \tag{4}$$

the magnetic and electric transition form factors

$$G_M(Q^2) \equiv F^*_1(Q^2) + F^*_2(Q^2),$$
$$G_E(Q^2) \equiv F^*_1(Q^2) - \frac{Q^2}{(M_{N_2} + M_{N_1})^2}F^*_2(Q^2), \tag{5}$$

and $\alpha$ is the fine-structure constant. Using these definitions, we can reconstruct $F^*_{1,2}$ from experimental values of helicity amplitudes.

## III. LATTICE SETUP

In this exploratory study, we will use an anisotropic lattice, that is, a lattice where the temporal lattice spacing is finer than the spatial ones. It has been demonstrated that for certain calculations, such as glueballs [20] and multiple excited-state masses [21], there are great advantages to using anisotropic over isotropic lattices even when the fundamental constituents are not heavy.

We perform our calculations on quenched[1] $16^3 \times 64$ lattices with anisotropy $\xi = 3$ (i.e. $a_s = 3a_t$), using Wilson gauge action with $\beta = 6.1$ and stout-link smeared [22] Sheikholeslami-Wohlert (SW) fermions [23] (with smearing parameters $\{\rho, n_\rho\} = \{0.22, 2\}$). The parameter $\nu$ is nonperturbatively tuned using the meson dispersion relation, and the clover coefficients are set to their tadpole-improved values. The inverse spatial lattice spacing is about 2 GeV, as determined by the static-quark potential, and the simulated pion mass is about 720 MeV. In total, we use 200 configurations of anisotropic lattices.

[1]A "quenched approximation" means the effective sea-quark mass is infinite. The quenched QCD (QQCD) is confining and asymptotically free, shows spontaneous chiral symmetry breaking, and differs from full QCD only in the relative weighting of the gauge configurations; it is reasonable to use quenched simulations to test new lattice techniques. QQCD is very useful for understanding and controlling sources of errors (except for those due to the quenched approximation) for a new methodology before it is extended to a much more expensive full-QCD calculation.

In this work, we will use the variational method and simultaneous fitting on two- and three-point Green functions to extract the $N$-$P_{11}$ transition form factors. The nucleon two-point correlators measured on the lattice are

$$\Gamma^{(2)}_{AB}(t; \vec{p}) = \sum_n \frac{E_n(\vec{p}) + M_n}{2E_n(\vec{p})} Z_{n,A}(\vec{p})Z_{n,B}(\vec{p})e^{-E_n(\vec{p})t}, \tag{6}$$

where the indices $A$ and $B$ denote different smearing parameters and $n$ runs over the basis of nucleon energy eigenstates; the states are defined to be normalized as $\langle 0|\chi^N|p, s\rangle = Z(\vec{p})u_s(\vec{p})$ with the nucleon interpolating field $\chi^N = \epsilon^{abc}(d^T_a C\frac{1+\gamma_4}{2}\gamma_5 u_b)u_c$; the spinors satisfy

$$\sum_s u_s(\vec{p})\bar{u}_s(\vec{p}) = \frac{E(\vec{p})\gamma^t - i\vec{\gamma}\cdot\vec{p} + M}{2E(\vec{p})}. \tag{7}$$

Traditionally, one is only interested in the ground state; thus the smearing parameters are chosen to overlap as little as possible with excited states. We will use various smearings to create correlators having appreciable overlap with the lowest nucleon radially excited state.

Similarly, the three-point function is

$$\Gamma^{(3),T}_{\mu,AB}(t_i, t, t_f, \vec{p}_i, \vec{p}_f) = \sum_n\sum_{n'} Z_V Z_{n',B}(\vec{p}_f)Z_{n,A}(\vec{p}_i) \times e^{-(t_f - t)E'_n(\vec{p}_f)}e^{-(t-t_i)E_n(\vec{p}_i)} \times \text{MEs}, \tag{8}$$

where $n$ and $n'$ label energy states and

$$\begin{aligned}\text{MEs} &= \sum_{s,s'} 4E_{n'}(\vec{p}_f)E_n(\vec{p}_i)T_{\alpha\beta}u_{n'}(\vec{p}_f, s')_\beta \\ &\quad\times\langle N_{n'}(\vec{p}_f, s')|V_\mu|N_n(\vec{p}_i, s)\rangle\bar{u}_n(\vec{p}_i, s)_\alpha \\ &= \text{Tr}[T\cdot(E_{n'}(\vec{p}_f)\gamma^t - i\vec{\gamma}\cdot\vec{p}_f + M_{n'})\cdot\text{FFs} \\ &\quad\cdot(E_n(\vec{p}_i)\gamma^t - i\vec{\gamma}\cdot\vec{p}_i + M_n)],\end{aligned} \tag{9}$$

where the projector is $T = \frac{1}{4}(1 + \gamma_4)(1 + i\gamma_5\gamma_3)$, $Z_V$ is the vector-current renormalization constant, and FF denotes the form factors. The vector current in Eq. (8) is $O(a)$ on-shell improved with the improved coefficient set to its tree-level value.[2] $Z_V$ is calculated nonperturbatively from the isovector vector charge $Z_V = 1/g^{u-d}_{V,\text{lat}}$. Note that when one calculates the three-point Green function in full QCD, there are two possible contraction topologies: "connected" and "disconnected" diagrams, when the vector-

[2]With smeared fermion actions, it has been seen on three-flavor anisotropic lattices with tree-level tadpole-improved coefficients in the fermion action that the nonperturbative coefficient conditions are satisfied without fine-tuning [24]. Similar behavior has also been observed in a quenched study [25], where the nonperturbative coefficients or renormalization constants in a smeared fermion action differed from tree-level values by a few percent.

current vertex appears on a vacuum bubble. In this work, only connected quantities are included.

## IV. NUMERICAL RESULTS

We apply a smearing function with gauge-invariant Gaussian form [26] to improve the overlap of fermion operators with states of interest. To obtain matrix elements involving states other than ground states, we need to be careful not to oversmear the fermions; a widely smeared fermion will greatly suppress excited-state signals. This goes against the standard practice used in the nucleon matrix elements where one increases the smearing parameters to suppress excited states. We use three Gaussian smearing parameters: $\sigma \in \{0.5, 2.5, 4.5\}$; the largest of these has excellent overlap with just the ground state, while the other two include substantial higher-state contributions. For both two-point and three-point correlators, we calculate all nine possible source-sink smearing combinations.

From the two-point functions, we wish to extract the energies ($E$'s) of at least the nucleon and $P_{11}$ and the matrix elements ($Z$'s) of our lattice operators between the vacuum and the baryon states at each momentum. We apply the variational method [27] to extract the best principal correlators corresponding to pure energy eigenstates from our matrix of correlators. A simple exponential fit to these yields $M_N = 1.48(2)$ GeV and $M_{P_{11}} = 2.53(8)$ GeV. We can check the quality of the fit using this simple form by examining the effective mass $[M_{\text{eff}}(t) = \ln(\Gamma^{(2)}(t+1)/\Gamma^{(2)}(t))]$, shown in Fig. 1. In our plateau region, there is no contamination from higher excited states. Figure 2 shows the dispersions of the nucleon and its first radially excited state; the slopes are consistent with the continuum value $c = 1$. The excited-state energies show better signal than those obtained using conventional isotropic lattices. The $Z$'s are then determined from the eigenvectors of the principal correlators; we select the eigenvectors from the time $t_Z$ that minimizes the discrepancy between the correlators reconstructed from our $Z$'s and $E$'s and the original two-point data. We find the mass of the negative-parity partner $S_{11}$ using the same method: $M_{S_{11}} = 2.40(10)$ GeV. This mass is lower than the $P_{11}$ mass due to the high quark masses used, a result consistent with previous lattice calculations; it is expected that the masses will cross when lower quark masses are used.

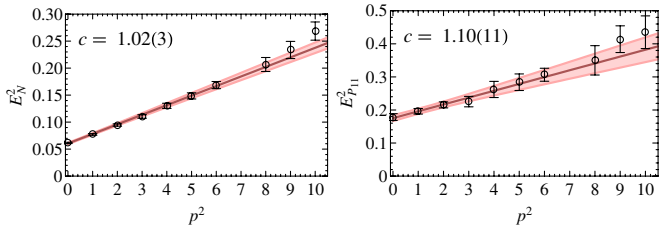


FIG. 2 (color online). Nucleon and $P_{11}$ dispersion relation. The vertical axis is in units of $a_t^{-2}$, while the horizontal axis is in units of $\frac{4\pi^2}{L_x^2} a_s^{-2}$ (where $L_x = 16$ is the length of the spatial dimension in lattice units). Linear fits to both sets of energies yield slopes consistent with the continuum value $c = 1$.

We calculate three-point functions with source and sink locations at 15 and 48, respectively. (This gives a source-sink separation of about 1.1 fm.) The final state always has zero momentum for convenience, while the momentum of the initial state varies but is always nonzero. We can get the nucleon form factors, $F_1^{NN}$ and $F_2^{NN}$, from the large Gaussian smearing ($\sigma = 4.5$) runs using a ratio approach [28]. We also apply the fitting method using the ground-state term of the fitting form in Eq. (8) on smearing parameter $\sigma = 4.5$ three-point correlators. The fit range is adjusted so that the fitted results are consistent under small perturbations to the range. We obtain nucleon-nucleon form factors $F_1$ and $F_2$ consistent with those derived from the ratio method, as shown in Fig. 3. Note that we not only get consistent numbers, but at large momenta, our fitting approach dramatically improves the signals. This is because when one tries to improve the

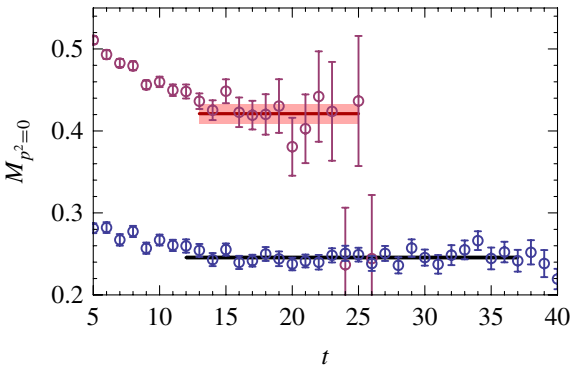


FIG. 1 (color online). Nucleon and $P_{11}$ effective masses. The vertical axis is in units of $a_t^{-1}$, while the horizontal axis is in units of $a_t$. The horizontal bars show the fit range and fitted values for each state.

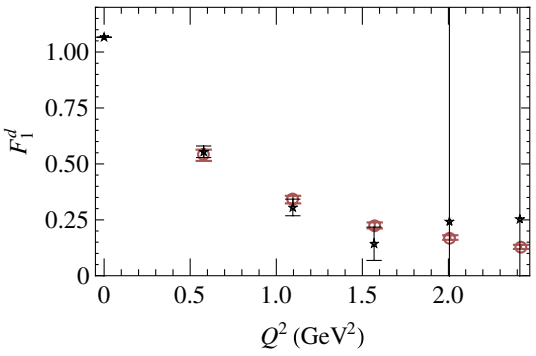


FIG. 3 (color online). Down-quark contribution to the nucleon Dirac form factor $F_1^d$ obtained from the ratio approach (stars) and the fitting method (circles).

ground-state signal, one introduces large smearing, which wipes out not only the excited states but also the higher-momentum states. Therefore, when one tries to project onto higher momenta, there is not much signal left, and noise dominates. Since we are considering excited states, we do not need such a strong smearing; therefore, the higher-momentum projections of the nucleon have improved signal. Since our pion mass is far heavier than the physical one, we do not expect to see very good agreement with experiment. As the pion mass approaches lighter values, the lattice data will trend toward the experimental values; for more details, see the recent review in Ref. [29].

The ratio method will not extract matrix elements beyond the ground state, but using the $Z$'s and $E$'s derived from our analysis of the two-point functions, we can extract excited matrix elements from the three-point functions by fitting to the form given in Eq. (8). We want to keep terms in Eq. (8) having $n$ and $n'$ running from the ground to the first excited state; thus, there would be four matrix elements in the minimum expansion, which will be free parameters in our fit. We increase the number of three-point correlators, first using just the diagonal correlators where the smearing is the same at the source and sink, and then using all nine smearing combinations. The nucleon-nucleon matrix elements are verified against the ratio method, and we check that the transition matrix elements are consistent between different sets. In the rest of this work, we show the results from the full 9-correlator simultaneous fits.

On the lattice, we can obtain both the form factors related to the Roper decay $P_{11} \rightarrow \gamma N$, and the one that is related to photoproduction, $\gamma^* N \rightarrow P_{11}$. A $P_{11}$ at rest has a $P$-wave decay into a pion and a nucleon and an $S$-wave decay into two pions and a nucleon via $S_{11}\pi$. Since we do not wish to consider the complicated case that occurs when two-particle states may be present, we must avoid kinematical situations in which decays can occur. In our simulation, these are suppressed by the high quark mass and discretization of momentum. However, our lowest-momentum $P_{11}$ ($E_{P_{11}} \approx 2.7$ GeV) can decay into a lowest-momentum pion ($E_\pi \approx 1.0$ GeV) and a nucleon at rest ($M_N \approx 1.5$ GeV). Since we cannot untangle the single-particle excited state from the two-particle state here, we drop this data point. All other decays are forbidden.

In Fig. 4, we show the transition form factors $F^*_{1,2}$ derived from experimental helicity amplitudes [15–19] and those from our numbers. In Fig. 5, we show the neutron-$P_{11}$ transition form factors with an experimental point. Note that since our nucleon and Roper masses are much higher than the physical ones, we are in the timelike region when we use the matrix element $\langle P_{11}|V_\mu|N\rangle$ to construct the transition form factors. As we decrease the pion mass, we will enter the spacelike region, and this matrix element will be helpful in giving us different $Q^2$

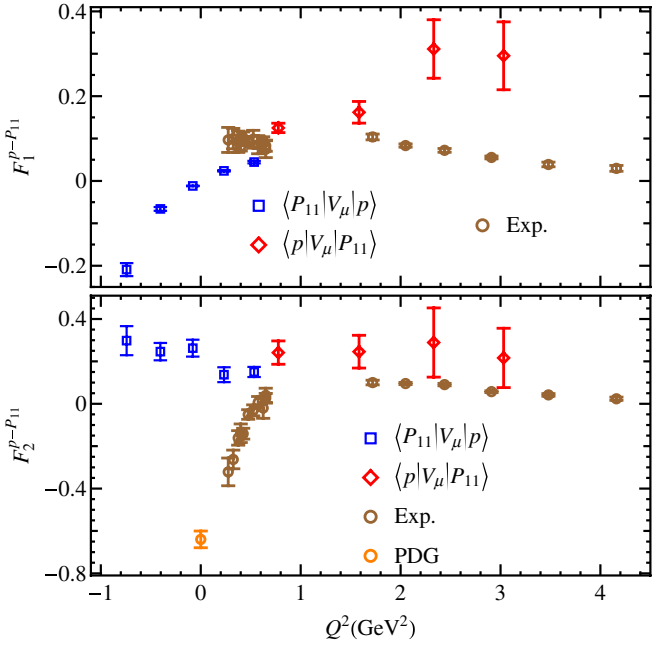


FIG. 4 (color online). Proton-Roper form factors $F^*_{1,2}$ obtained from CLAS experiments [15–19] and the PDG [30] number (circles) and our fitting method (squares, diamonds).

points. Our calculation seems to be quite different from the experimental values. This is somewhat expected, since our pion mass is much heavier than the physical value. Even in unquenched calculations, the nucleon form factors do not agree with experimental values with a pion mass as low as 300 MeV [29]. We will see whether the lattice data ap-

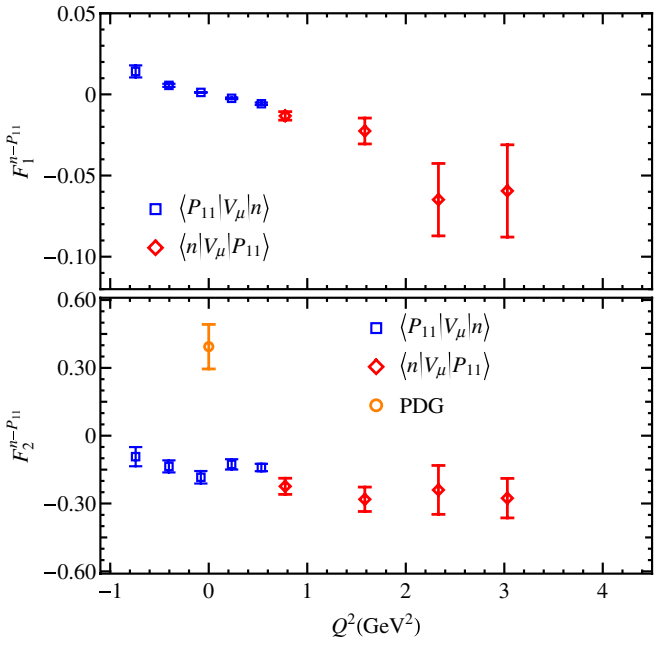


FIG. 5 (color online). Neutron-Roper form factors $F^*_{1,2}$ obtained from the PDG [30] number (circle) and our fitting method (squares, diamonds).

proach experiment as the pion mass used is decreased in future calculations.

## V. CONCLUSION AND OUTLOOK

This exploratory study demonstrates that the ground-radially excited transition form factors can be measured in the nucleon system from a first-principles lattice calculation. Using the fitting approach with appropriately chosen operator smearing, we not only improve the signal in the nucleon-nucleon form factors (especially at large momenta), but also successfully extract the nucleon-$P_{11}$. We may vary the projector used in the three-point function to further improve the signal. In the future, since the pion mass in our simulation is very heavy at 720 MeV, we will consider lighter pion masses as well as start work on unquenched anisotropic lattices.

## ACKNOWLEDGMENTS

This work was done using the CHROMA software suite [31] on clusters at Jefferson Laboratory using time awarded under the SciDAC Initiative. This work was supported by DOE Contract No. DE-AC05-06OR23177, under which Jefferson Science Associates, LLC, operates Jefferson Lab.

[1] T. S. H. Lee and L. C. Smith, J. Phys. G **34**, S83 (2007).
[2] A. Matsuyama, T. Sato, and T. S. H. Lee, Phys. Rep. **439**, 193 (2007).
[3] C. E. Carlson and N. C. Mukhopadhyay, Phys. Rev. Lett. **67**, 3745 (1991).
[4] O. Krehl, C. Hanhart, S. Krewald, and J. Speth, Phys. Rev. C **62**, 025207 (2000).
[5] S. Sasaki, T. Blum, and S. Ohta, Phys. Rev. D **65**, 074503 (2002).
[6] D. Guadagnoli, M. Papinutto, and S. Simula, Phys. Lett. B **604**, 74 (2004).
[7] D. B. Leinweber, W. Melnitchouk, D. G. Richards, A. G. Williams, and J. M. Zanotti, Lect. Notes Phys. **663**, 71 (2005).
[8] K. Sasaki, S. Sasaki, and T. Hatsuda, Phys. Lett. B **623**, 208 (2005).
[9] K. Sasaki and S. Sasaki, Phys. Rev. D **72**, 034502 (2005).
[10] T. Burch *et al.*, Phys. Rev. D **74**, 014504 (2006).
[11] N. Mathur *et al.*, Phys. Lett. B **605**, 137 (2005).
[12] S. Capstick and W. Roberts, Prog. Part. Nucl. Phys. **45**, S241 (2000).
[13] I. G. Aznauryan, Phys. Rev. C **76**, 025212 (2007).
[14] P. Maris and C. D. Roberts, Int. J. Mod. Phys. E **12**, 297 (2003).
[15] V. I. Mokeev and V. D. Burkert, AIP Conf. Proc. **842**, 339 (2006).
[16] K. Joo *et al.* (CLAS Collaboration), Phys. Rev. C **72**, 058202 (2005).
[17] V. D. Burkert and T. S. H. Lee, Int. J. Mod. Phys. E **13**, 1035 (2004).
[18] V. D. Burkert, Eur. Phys. J. A **17**, 303 (2003).
[19] I. Aznauryan and V. Burkert, arXiv:0711.1120.
[20] C. J. Morningstar and M. J. Peardon, Phys. Rev. D **60**, 034509 (1999).
[21] S. Basak *et al.*, arXiv:hep-lat/0609052.
[22] C. Morningstar and M. J. Peardon, Phys. Rev. D **69**, 054501 (2004).
[23] B. Sheikholeslami and R. Wohlert, Nucl. Phys. **B259**, 572 (1985).
[24] H.-W. Lin, R. G. Edwards, and B. Joo, Proc. Sci., LAT2007 (2007) 119 [arXiv:0709.4680].
[25] R. Hoffmann, A. Hasenfratz, and S. Schaefer, Proc. Sci., LAT2007 (2007) 104 [arXiv:0710.0471].
[26] S. Gusken, Nucl. Phys. B, Proc. Suppl. **17**, 361 (1990).
[27] M. Luscher and U. Wolff, Nucl. Phys. **B339**, 222 (1990).
[28] P. Hagler *et al.* (LHPC), Phys. Rev. D **68**, 034505 (2003).
[29] C. F. Perdrisat, V. Punjabi, and M. Vanderhaeghen, Prog. Part. Nucl. Phys. **59**, 694 (2007).
[30] W. M. Yao *et al.* (Particle Data Group), J. Phys. G **33**, 1 (2006).
[31] R. G. Edwards and B. Joo (SciDAC), Nucl. Phys. B, Proc. Suppl. **140**, 832 (2005).